International Journal Of
Industrial Electronics Control and Optimization
Print ISSN: 3517-2645
Online ISSN: 3568-2645
Homepage: https://ieco.usb.ac.ir/

A Chaotic Adaptive Quantum-Inspired GBMO Optimization for Precise Parameter Extraction of Photovoltaic Models

Elaheh Gharibshahian1

Department of Basic Science, Technical and Vocational university, Tehran, Iran[1]
Corresponding author's email: egharibshahian@tvu.ac.ir

Article Info

Article type:
Research Article

Article history:
Received: **********
Received in revised form: **********
Accepted: **********
Published online: **********

Keywords:
Photovoltaic parameter estimation,
quantum-inspired optimization,
chaotic maps, adaptive control,
double-diode model

ABSTRACT

This paper presents a novel Chaotic Adaptive Quantum-Inspired Gases Brownian Motion Optimization (CAQI-GBMO) algorithm for accurate parameter estimation of photovoltaic models. The proposed method addresses the fundamental challenge of balancing exploration and exploitation in metaheuristic optimization by integrating three complementary mechanisms: quantum behavior modeling enables particles to maintain population diversity through probabilistic position distributions; multiple chaotic maps enhance search space coverage with superior statistical properties; and adaptive parameter control dynamically adjusts exploration-exploitation balance throughout the optimization process. The algorithm is specifically designed for the double-diode model parameter estimation problem, which involves seven unknown parameters with strong correlations and a multimodal objective function landscape. Experimental validation using benchmark R.T.C. France solar cell data demonstrates that CAQI-GBMO achieves a minimum RMSE of $9.824708 \times 10^{-4}$for the double-diode model, matching the best-known results with superior consistency across 5000 independent runs. Comparative analysis against state-of-the-art algorithms, including SENMSSA, iAPO, and IWSO, reveals that CAQI-GBMO achieves the lowest Friedman ranking of 1.62, indicating statistically significant performance improvements. The accurate parameter estimates enable precise reproduction of current-voltage and power-voltage characteristics, which are essential for maximum power point tracking, system simulation, and performance optimization in practical photovoltaic installations.

I. Introduction

1. 1. Background and Motivation

The global energy landscape is undergoing a profound transformation driven by the urgent need to address climate change and transition toward sustainable energy systems [1]. Fossil fuels, which have historically powered industrial development, are increasingly recognized as finite resources with devastating environmental consequences. The power sector alone accounts for approximately 35% of global carbon emissions, making it a critical target for decarbonization efforts [2]. In response, nations worldwide are accelerating their transition to renewable energy sources, with solar photovoltaic technology emerging as a cornerstone of this transformation [3].

Solar energy offers unparalleled advantages among renewable sources due to its abundance, accessibility, and decreasing implementation costs [4]. Unlike conventional power generation methods, solar PV systems can be deployed at various scales, making them adaptable to diverse geographical and economic contexts. Projections indicate that by 2040, global PV capacity will reach 4240 GW, representing a staggering increase from installations in the early 2000s [5]. This exponential growth underscores the critical importance of optimizing PV system performance to maximize energy yield and ensure economic viability.

The efficiency of solar cells depends on numerous factors, including material properties, manufacturing quality, and operating conditions such as irradiance and temperature [6]. Under real-world conditions, these factors interact in complex ways that are not fully captured by simplified analytical models. Accurate modeling of PV cell behavior requires precise estimation of internal parameters that govern current-voltage and power-voltage characteristics. These parameters—including photogenerated current, saturation currents, series and shunt resistances, and diode ideality factors—are not directly measurable but must be inferred from experimental data through parameter estimation techniques [7]. The parameter estimation problem for PV models is inherently challenging due to several factors. First, the governing equations are implicit and transcendental, lacking closed-form analytical solutions [8]. Second, the objective function landscape is characterized by multiple local optima, nonlinearities, and strong parameter interactions. Third, experimental measurements contain noise and uncertainties that complicate the identification process. These characteristics make PV parameter estimation a multimodal, nonlinear inverse problem that demands sophisticated optimization approaches [9].

1.2. Photovoltaic Cell Modeling

The electrical behavior of solar cells is commonly represented through equivalent circuit models of varying complexity. The single-diode model remains the most widely adopted representation due to its simplicity and computational efficiency, comprising five unknown parameters: photogenerated current, diode saturation current, series resistance, shunt resistance, and diode ideality factor [10]. Despite its widespread use, the SDM exhibits limitations in accurately representing PV behavior under low-irradiance conditions, where recombination effects in the depletion region become significant [11].

To address these limitations, the double-diode model incorporates an additional diode to account for recombination current losses [12]. The DDM introduces two additional parameters—a second saturation current and a second ideality factor—resulting in seven unknown parameters that must be estimated. The additional complexity enables more accurate representation of PV characteristics across a wider range of operating conditions, particularly at low voltages and under partial shading [13]. However, the increased dimensionality also exacerbates the challenges associated with parameter estimation, creating a more rugged objective function landscape with enhanced susceptibility to local optima trapping.

The three-diode model adds a third diode. It models grain boundary and leakage currents in polycrystalline and thin-film technologies [14]. While offering the highest accuracy among lumped-parameter models, the TDM's nine unknown parameters present an even more formidable optimization challenge. The choice among these models involves a fundamental trade-off between accuracy and identifiability, with higher-dimensional models offering improved fidelity at the cost of increased estimation difficulty.

1.3. Review of Parameter Estimation Approaches

Parameter estimation techniques for PV models can be broadly categorized into three classes: analytical methods, deterministic numerical methods, and metaheuristic optimization algorithms [15]. Analytical approaches derive parameter values directly from key points on the I-V curve, such as short-circuit, open-circuit, and maximum power points. While computationally efficient, these methods rely on simplifying assumptions that compromise accuracy and fail to capture the full nonlinear behavior of PV devices [16].

Deterministic numerical methods, such as Newton-Raphson and Levenberg-Marquardt, formulate the parameter estimation problem as a system of equations. This system is then solved through iterative procedures. These methods require differentiable objective functions and convex search spaces—conditions rarely satisfied in PV parameter estimation. Moreover, deterministic methods are highly sensitive to initial value assumptions, with poor initialization often leading to divergence or convergence to suboptimal solutions [17].

Metaheuristic optimization algorithms have emerged as the dominant paradigm for PV parameter estimation due to their ability to navigate complex, nonlinear, and multimodal search spaces without requiring gradient information [18]. These nature-inspired algorithms balance exploration of the solution space with exploitation of promising regions, enabling effective identification of near-optimal parameter sets. The literature documents numerous successful applications of metaheuristic algorithms to PV parameter estimation, each offering unique advantages and facing distinct limitations [19,20,21].

Particle Swarm Optimization and its variants have been extensively applied to PV parameter estimation [22]. Quantum-behaved Particle Swarm Optimization overcomes certain limitations by applying quantum mechanics principles. This enables particles to occupy any position in the search space with defined probability densities. Consequently, global convergence is theoretically guaranteed [23]. Differential Evolution and its enhanced variants incorporating adaptive parameter control and

opposition-based learning have achieved state-of-the-art results on benchmark PV problems [24].

The Salp Swarm Algorithm, inspired by the chain-forming behavior of salps, has been applied with promising results [25]. However, the basic SSA exhibits limited exploration capability and frequently stagnates in local optima when confronted with complex objective functions. Enhanced variants, such as the Super-Evolutionary Nelder-Mead Salp Swarm Algorithm, combine Gaussian-Cauchy mutation and vertical-horizontal crossover with the Nelder-Mead simplex method. This integration yields competitive performance. The algorithm has been applied to estimate parameters for SDM, DDM, and TDM [26]. The Whale Optimization Algorithm and its hybrid variants have shown improved accuracy and reliability for PV applications [27]. Similarly, the Grey Wolf Optimizer and Harris Hawks Optimizer have demonstrated effectiveness in balancing exploration and exploitation. However, like other metaheuristic algorithms, these methods remain susceptible to premature convergence and exhibit performance degradation on problems with complex parameter interactions [28]. Recent years have witnessed increasingly sophisticated algorithms for PV parameter estimation. The Artificial Protozoa Optimizer, inspired by Euglena behavior, offers a novel framework for balancing exploration and exploitation [29]. An improved version, iAPO, incorporates random neighbor-pair sampling and enhanced movement strategies to achieve superior performance in SDM and DDM parameter estimation [30]. The White Shark Optimizer has been enhanced through opposition-based learning and chaos theory to improve convergence characteristics [31].

Despite these advances, significant challenges persist. Many algorithms exhibit inconsistent performance across different PV models and operating conditions [32]. The trade-off between exploration and exploitation remains difficult to optimize, with algorithms either converging prematurely or failing to refine solutions with sufficient precision. Computational efficiency becomes increasingly important as PV systems scale and require real-time parameter adaptation. Additionally, the stochastic nature of metaheuristic algorithms introduces variability in results, complicating reliability assessment.

1.4. Research Gap and Proposed Approach

A critical examination of the literature reveals persistent gaps that motivate this research. Existing metaheuristic algorithms, while effective in many scenarios, share common limitations that constrain their performance. The fundamental challenge lies in achieving an optimal balance between global exploration—identifying promising regions in the solution space—and local exploitation—refining solutions with high precision [33]. Algorithms biased toward exploration exhibit slow convergence and may fail to identify optimal parameters within reasonable computational budgets. Conversely, algorithms emphasizing exploitation risk premature convergence to local optima, yielding suboptimal parameter estimates.

The quantum-inspired paradigm offers a promising avenue for addressing these limitations. By modeling search agents with quantum behavior, algorithms can maintain population diversity while simultaneously converging toward optimal solutions [34]. Quantum-behaved particles possess inherent uncertainty in their positions. This allows for thorough exploration while preserving the capacity to exploit promising regions. Exploitation occurs via measurement operations. The Gases Brownian Motion Optimization algorithm, inspired by the random motion of gas molecules, provides an alternative framework for balancing exploration and exploitation through temperature-controlled search behavior [35,21].

Chaos theory presents another powerful mechanism for improving metaheuristic algorithms. Chaotic maps generate sequences that are deterministic yet exhibit pseudo-random properties with enhanced statistical characteristics compared to pseudo-random number generators [36]. Incorporating chaotic sequences into optimization algorithms can improve exploration by enabling more thorough coverage of the solution space while maintaining deterministic structure necessary for reproducible results.

Adaptive parameter control represents a third dimension for algorithm enhancement. Metaheuristic algorithms typically employ fixed parameter values that may not optimally balance exploration and exploitation throughout the search process [37]. Adaptive mechanisms that adjust algorithm parameters based on search progress can significantly improve performance by maintaining appropriate exploration-exploitation balance at each stage.

Based on these observations, this paper proposes a novel Chaotic Adaptive Quantum-Inspired Gases Brownian Motion Optimization algorithm for photovoltaic parameter estimation. The proposed approach integrates three complementary enhancement mechanisms within a unified optimization framework. First, search agents are endowed with quantum mechanical properties, enabling them to appear anywhere in the search space with probability densities governed by wave functions. This quantum behavior facilitates global exploration while maintaining the potential for precise localization through measurement operations.

Second, multiple chaotic maps are employed to generate sequences that guide search behavior throughout the optimization process. The chaotic dynamics enhance exploration by providing deterministic yet statistically superior coverage of the solution space. Different chaotic

maps are evaluated to identify those most effective for PV parameter estimation, with adaptive selection mechanisms determining the most appropriate map at each search stage.

Third, algorithm parameters governing quantum behavior, chaotic dynamics, and Brownian motion are continuously adjusted based on search progress metrics. This adaptive control ensures that the algorithm maintains an optimal exploration-exploitation balance throughout the search, transitioning from broad exploration in early iterations to refined exploitation in later stages.

The CAQI-GBMO algorithm is specifically designed to address the challenges of parameter estimation for the double-diode model, in which seven strongly correlated unknown parameters must be accurately identified from noisy experimental data. The proposed approach leverages quantum behavior to maintain population diversity in the high-dimensional search space, chaotic maps to enhance exploration efficiency, and adaptive control to ensure timely convergence to high-precision solutions.

1.5. Paper Organization

The remainder of this paper is organized as follows: Section 2 presents the mathematical modeling of photovoltaic systems, including formulations of the single-diode, double-diode, and three-diode models, as well as the objective function for parameter estimation. Section 3 describes the proposed Chaotic Adaptive Quantum-Inspired Gases Brownian Motion Optimization algorithm in detail, including the quantum behavioral model, chaotic map integration mechanisms, adaptive parameter control strategies, and the complete algorithmic framework. Section 4 presents the experimental setup, including benchmark datasets, parameter ranges, evaluation metrics, comparison algorithms, and comprehensive experimental results and analysis. Section 5 concludes the paper with a summary of key contributions and findings.

2. Photovoltaic Cell Modeling and Problem Formulation

Accurate mathematical modeling of photovoltaic cells is essential for understanding their electrical behavior, optimizing performance, and enabling maximum power point tracking in practical applications. This section presents the equivalent circuit models commonly used to represent PV cells. These include the single-diode and double-diode models. The photovoltaic module model is also presented. The mathematical formulations, parameter definitions, and objective functions for parameter estimation are systematically described.

2.1 Single-Diode Model

The single-diode model is the most widely adopted representation for photovoltaic cells due to its simplicity and reasonable accuracy under standard operating conditions. The SDM originates from Shockley's diode theory. It captures the essential I-V characteristics of p-n junctions while preserving computational tractability. Figure 1 illustrates the equivalent circuit of the SDM, comprising five key components: a photogenerated current source, a single diode representing the p-n junction, a series resistance accounting for bulk and contact resistances, and a shunt resistance representing leakage currents across the junction.

The output current of the SDM is derived by applying Kirchhoff's current law to the equivalent circuit. The photogenerated current I_{ph} represents the current generated by incident light absorption, which is proportional to irradiance and cell area. A portion of these current flows through the diode (I_d), another portion through the shunt resistance (I_{sh}), and the remainder constitutes the load current (I_L) delivered to the external circuit. The relationship among these currents is expressed as:

$$I_L = I_{ph} - I_d - I_{sh} \quad (1)$$

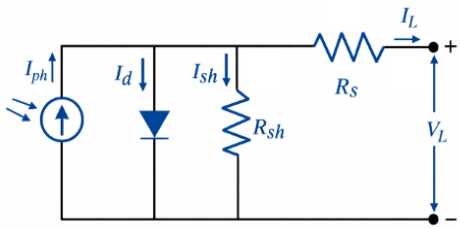

Figure. 1. Equivalent circuit diagram of the single-diode model showing the photogenerated current source (I_{ph}), diode (D), series resistance (R_s), and shunt resistance (R_{sh}).

The diode current I_d is described by the Shockley equation, which models the nonlinear behavior of the p-n junction. This current depends on the voltage across the diode, which equals the sum of the load voltage and the voltage drop across the series resistance. The mathematical expression is:

$$I_d = I_{sd}\left[exp\left(\frac{q(V_L+R_sI_L)}{nkT}\right) - 1\right] \quad (2)$$

where I_{sd} represents the diode reverse saturation current, q is the electron charge ($1.60217646 \times 10^{-19}$ C), n is the diode ideality factor, k is Boltzmann's constant ($1.3806503 \times 10^{-23}$ J/K), and T is the cell temperature in Kelvin. The ideality factor typically ranges between 1 and 2, with values closer to 1 indicating ideal diode behavior dominated by diffusion current, while higher values indicate recombination effects.

The shunt-resistance current is calculated using Ohm's law in the parallel-resistance branch. The voltage across

the shunt resistance is identical to the voltage across the diode, yielding:

$$I_{sh} = \frac{V_L + R_s I_L}{R_{sh}} \quad (3)$$

Substituting Equations (2) and (3) into Equation (1) yields the complete implicit equation relating output current to output voltage for the SDM:

$$I_L = I_{ph} - I_{sd}\left[exp\left(\frac{q(V_L + R_s I_L)}{nkT}\right) - 1\right] - \frac{V_L + R_s I_L}{R_{sh}} \quad (4)$$

Equation (4) is implicit because the current appears on both sides, including within the exponential term and the shunt resistance expression. This implicitness necessitates numerical solution methods for calculating the current at any given voltage. The SDM contains five unknown parameters that must be estimated from experimental data: the photogenerated current, the diode saturation current, the series resistance, the shunt resistance, and the diode ideality factor n. Accurate estimation of these parameters is crucial for reliable PV system simulation and performance prediction.

2.2 Double-Diode Model

While the SDM provides adequate accuracy under many operating conditions, it exhibits limitations in representing PV behavior at low irradiance levels and near the open-circuit voltage. These limitations arise because the SDM does not explicitly account for recombination losses in the depletion region. The double-diode model addresses this deficiency by incorporating an additional diode to model recombination current, resulting in improved accuracy across a wider range of operating conditions. Figure 2 presents the equivalent circuit of the DDM.

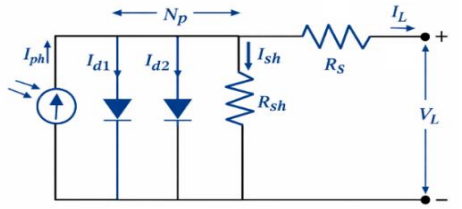

Figure. 2. Equivalent circuit diagram of the double-diode model showing the photogenerated current source (I_{ph}), two diodes (D_1 and D_2) representing diffusion and recombination currents, series resistance (R_s), and shunt resistance (R_{sh}).

The DDM includes two parallel diodes: diode D_1 models the diffusion current in the quasi-neutral regions, while diode D_2 accounts for recombination current in the depletion region. Each diode has its own saturation current and ideality factor, enabling more flexible fitting of the I-V characteristics. The output current equation for the DDM is derived similarly to the SDM but includes two diode current terms:

$$I_L = I_{ph} - I_{d1} - I_{d2} - I_{sh} \quad (5)$$

The two diode currents are expressed using Shockley equations with distinct parameters:

$$I_{d1} = I_{sd1}\left[exp\left(\frac{q(V_L + R_s I_L)}{n_1 kT}\right) - 1\right] \quad (6)$$

$$I_{d2} = I_{sd2}\left[exp\left(\frac{q(V_L + R_s I_L)}{n_2 kT}\right) - 1\right] \quad (7)$$

where I_{sd1} and I_{sd2} are the saturation currents of the first and second diodes, respectively, and n_1 and n_2 are their corresponding ideality factors. The shunt current, Ish, remains as defined in Equation (3). Substituting these expressions into Equation (5) yields the complete DDM equation:

$$I_L = I_{ph} - I_{sd1}\left[exp\left(\frac{q(V_L + R_s I_L)}{n_1 kT}\right) - 1\right] - I_{sd2}\left[exp\left(\frac{q(V_L + R_s I_L)}{n_2 kT}\right) - 1\right] - \frac{V_L + R_s I_L}{R_{sh}} \quad (8)$$

Relative to the SDM, the DDM includes two additional unknown parameters, which result in a total of seven parameters that require estimation: I_{ph}, I_{sd1}, I_{sd2}, R_s, R_{sh}, n_1, and n_2. The increased parameter dimensionality enhances model flexibility but simultaneously complicates the estimation problem due to stronger parameter correlations and a more complex objective function landscape.

2.3 Photovoltaic Module Model

Practical photovoltaic systems employ modules consisting of multiple solar cells connected in series and parallel configurations to achieve desired voltage and current ratings. While individual cell models can be scaled to represent modules, the module-level model must account for the interconnection topology. Figure 3 illustrates the equivalent circuit of a PV module comprising Ns cells in series and Np cells in parallel.

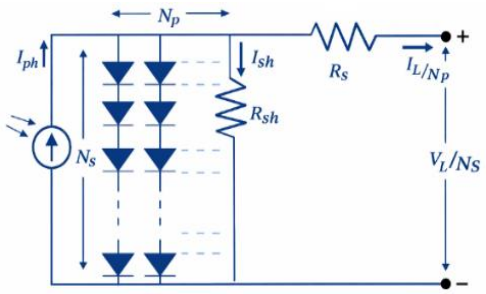

Figure. 3. Equivalent circuit diagram of a photovoltaic module showing series and parallel interconnection of individual solar cells.

For a module with Ns series-connected cells and Np parallel-connected strings, the output current equation is derived by scaling the single-diode model. The module output current I_L_module is related to the individual cell current by the parallel configuration, while the module voltage V_L_module is related to the cell voltage by the series configuration. The resulting equation is:

$$I_L = N_p I_{ph} - N_p I_{sd}\left[exp\left(\frac{q(V_L/N_s+R_s I_L/N_p)}{nkT}\right)-1\right] - \frac{N_p V_L/N_s+R_s I_L}{R_{sh}} \quad (9)$$

Equation (9) assumes that all cells in the module are identical and operating under uniform conditions. An assumption that may be violated under partial shading or non-uniform temperature distributions. Nevertheless, this model provides a practical representation for most engineering applications. The parameters to be estimated for the PV module model are the same five parameters as the SDM, but they now represent the equivalent cell-level parameters after accounting for the module configuration.

2.4 Objective Function Formulation

The parameter estimation problem for PV models aims to determine the optimal parameter vector X that minimizes the discrepancy between measured and model-predicted current values across a set of experimental data points. This discrepancy is quantified using an appropriate error metric, with the root mean square error being the most commonly employed criterion due to its sensitivity to large errors and its ability to reflect overall fitting accuracy.

For a given experimental dataset consisting of N pairs of voltage and current measurements $(V_i, I_{meas,i})$, the RMSE is defined as:

$$RMSE(X) = \sqrt{\frac{1}{N}\sum_{i=1}^{N} f\,(V_i, I_{meas,i}, X)^2} \quad (10)$$

where f(V, I, X) represents the error function for the specific PV model under consideration. For the SDM, the error function is derived directly from Equation (4):

$$f_{SD}(V, I, X) = I_{ph} - I_{sd}\left[exp\left(\frac{q(V+R_s I)}{nkT}\right)-1\right] - \frac{V+R_s I}{R_{sh}} - I_{meas} \quad (11)$$

The parameter vector for SDM is X = [I_{ph}, I_{sd}, R_s, R_{sh}, n]. For the DDM, the error function follows from Equation (8):

$$f_{DD}(V, I, X) = I_{ph} - I_{sd1}\left[exp\left(\frac{q(V+R_s I)}{n_1 kT}\right)-1\right] - I_{sd2}\left[exp\left(\frac{q(V+R_s I)}{n_2 kT}\right)-1\right] - \frac{V+R_s I}{R_{sh}} - I_{meas} \quad (12)$$

with parameter vector X = [I_{ph}, I_{sd1}, I_{sd2}, R_s, R_{sh}, n_1, n_2]. For the PV module model, the error function based on Equation (9) is:

$$f_{PV}(V, I, X) = N_p I_{ph} - N_p I_{sd}\left[exp\left(\frac{q(V/N_s+R_s I/N_p)}{nkT}\right)-1\right] - \frac{N_p V/N_s+R_s I}{R_{sh}} - I_{meas} \quad (13)$$

Equations (11)-(13) are implicit in the measured current I_{meas}, requiring numerical solution to evaluate the error function at each data point. The implicit nature of these equations arises because the current appears both in the exponential terms and in the shunt resistance expression. For a given parameter vector X and voltage V, the corresponding model-predicted current I_{calc} must be obtained by numerically solving the implicit equation. This is typically accomplished using iterative methods such as the Newton-Raphson algorithm or by reformulating the equation using Lambert W functions. The parameter estimation problem is thus a nonlinear optimization problem with the following characteristics: (1) the objective function is multimodal, containing multiple local minima; (2) the parameters exhibit strong correlations, making the problem ill-conditioned; (3) the objective function is computationally expensive to evaluate due to the need for numerical solution of implicit equations at each data point; and (4) experimental measurements contain noise and uncertainties that complicate the identification process. These characteristics necessitate the use of robust optimization algorithms that can navigate complex search spaces while maintaining computational efficiency. The search space for parameter estimation is defined by physically meaningful bounds on each parameter. Typical bounds are: photogenerated current between 0 and 1A; saturation currents between 0 and 1 μA; series resistance Rs between 0 and 0.5 Ω; shunt resistance between 0 and 100 Ω; and ideality factors N, N1, N2 between 1 and 2. These bounds ensure that the estimated parameters correspond to physically realizable values while providing sufficient search space for the optimization algorithm.

In summary, the PV parameter estimation problem is to determine the parameter vector X that minimizes RMSE(X) subject to bounds on each parameter. The problem is challenging due to the nonlinear, implicit, and multimodal nature of the objective function, as well as the correlations among parameters. The following sections present a novel optimization algorithm designed to address these challenges effectively.

3. Proposed Chaotic Adaptive Quantum-Inspired GBMO Algorithm

This section presents the proposed Chaotic Adaptive Quantum-Inspired Gases Brownian Motion Optimization

(CAQI-GBMO) algorithm for photovoltaic parameter estimation. The algorithm integrates three complementary enhancement mechanisms within a unified optimization framework: quantum behavior modeling, chaotic map integration, and adaptive parameter control. Each mechanism is designed to address specific limitations of conventional metaheuristic algorithms, particularly the challenges of premature convergence and inadequate exploration-exploitation balance in complex multimodal search spaces.

3.1 Foundation of Gases Brownian Motion Optimization

The Gases Brownian Motion Optimization algorithm is inspired by the random motion of gas molecules within a confined space. In kinetic theory, gas molecules move randomly. They collide with each other and with the container walls. These collisions gradually bring the system to equilibrium states. This behavior offers a useful metaphor for optimization. Molecules represent candidate solutions. They explore the search space through Brownian motion. They interact with each other via collision dynamics. In the standard GBMO framework, each gas molecule is characterized by its position vector $X_i = (X_i^1, X_i^2, X_i^3, \dots, X_i^D)$ in a D-dimensional search space, In the standard GBMO framework, each gas molecule is characterized by its position vector in a D-dimensional search space, where D is the number of parameters to be estimated. The molecules also possess velocity vectors V_i that determine their movement. The temperature T of the system controls the intensity of molecular motion, with higher temperatures promoting exploration and lower temperatures favoring exploitation. The movement of molecules is governed by Brownian motion principles, where each molecule's position update incorporates both deterministic and stochastic components. The temperature parameter decreases progressively throughout the optimization process, analogous to annealing in physical systems, enabling the transition from global exploration to local exploitation. However, the standard GBMO algorithm exhibits limitations in maintaining population diversity and may converge prematurely when applied to complex multimodal problems such as PV parameter estimation.

3.2 Quantum Behavior Modeling

The first improvement to the GBMO framework integrates the principles of quantum behavior into molecular dynamics. In classical mechanics, particles follow deterministic trajectories determined by initial conditions and forces. In contrast, quantum mechanics introduces inherent uncertainty, with particles described by probability density functions rather than definite positions. This quantum uncertainty provides a powerful mechanism for maintaining population diversity and enabling escape from local optima.

In the proposed CAQI-GBMO algorithm, each gas molecule is treated as a quantum particle characterized by a wave function $\psi(x,t)$ rather than a definite position. The probability density of finding a quantum particle at position x is given by $|\psi(x,t)|^2$. Drawing on quantum-behaved particle swarm optimization, we model quantum behavior using a Delta potential well. Each molecule oscillates in a well centered at an attractor pi, it blends the individual's best and the swarm's best.

The wave function for a quantum particle in a one-dimensional delta well can be solved analytically, yielding an exponential probability distribution. For multidimensional problems, the position of each quantum particle is updated using the Monte Carlo method:

$$X_i^{t+1} = p_i^t \pm \frac{L_i^t}{2} ln\left(\frac{1}{u}\right) (14)$$

where u is a random number uniformly distributed in (0,1), and the sign ± is chosen randomly with equal probability. The parameter L_i^tdetermines the search range of the quantum particle and is calculated as:

$$L_i^t = 2\beta |m_i^t - X_i^t| (15)$$

where β is the contraction-expansion coefficient, and $m_i^t$is the mean best position computed as the average of all personal best positions:

$$m_i^t = \frac{1}{N}\sum_{j=1}^{N} p_j^t (16)$$

The attractor point $p_i^t$is a stochastic combination of the particle's personal best and the global best:

$$p_i^t = \frac{\varphi_1 p_i^t + \varphi_2 g^t}{\varphi_1 + \varphi_2} (17)$$

where φ_1 and φ_2 are random numbers uniformly distributed in (0,1), p_i^t is the personal best position of particle i, and $g^t$is the global best position found so far.

The quantum behavior mechanism enables particles to appear anywhere in the search space with probability densities that favor regions near the attractor while maintaining a nonzero probability of exploring distant regions. This property is crucial for escaping local optima and maintaining population diversity throughout the optimization process.

3.3 Integration of Chaotic Maps

The second enhancement involves incorporating chaotic maps to improve the algorithm's exploration efficiency and convergence characteristics. Chaotic systems are deterministic dynamical systems that exhibit pseudo-random behavior and sensitive dependence on initial conditions.

Chaotic maps produce sequences with superior statistical properties compared to pseudo-random number generators. These sequences exhibit better uniformity. They also have higher entropy. Furthermore, they show a greater ability to escape cycles. In the CAQI-GBMO algorithm, multiple chaotic maps are employed to generate sequences that guide various stochastic processes within the optimization framework. The choice of a chaotic map can significantly influence algorithm performance, and we evaluate several well-known maps to identify those most effective for PV parameter estimation.The logistic map is one of the simplest and most widely studied chaotic systems, defined as:

$$z_{k+1} = \mu z_k(1 - z_k) \quad (18)$$

where $z_k \in (0,1)$ and μ is the control parameter. For μ = 4, the system exhibits fully chaotic behavior, generating sequences that uniformly cover the interval (0,1). The tent map is another piecewise linear chaotic map defined as:

$$z_{k+1} = \begin{cases} \frac{z_k}{0.7} & z_k < 0.7 \\ \frac{1-z_k}{0.3} & z_k \geq 0.7 \end{cases} \quad (19)$$

The tent map produces sequences with good statistical properties and is computationally efficient.

The sine map is defined as:

$$z_{k+1} = \frac{\alpha}{4} sin(\pi z_k) \quad (20)$$

where α is a control parameter typically set to 4 to achieve chaotic behavior. The Gaussian map is defined as:

$$z_{k+1} = exp(-\alpha z_k^2) + \zeta \quad (21)$$

where α and ζ are parameters controlling the chaotic dynamics. In the proposed algorithm, chaotic sequences replace pseudo-random numbers. This replacement occurs in critical stochastic operations. These operations include the initial setting of particle positions. They also include the generation of quantum probabilities. Furthermore, they include the selection of mutation strategies. For each operation, a specific chaotic map is selected based on its statistical properties and suitability for the task. The chaotic sequences are generated as:

$$z_{k+1} = CM(z_k, \lambda) \quad (22)$$

where CM represents the chosen chaotic map with control parameter λ. The chaotic variable z_k is then mapped to the desired range using appropriate transformations.

The integration of chaotic maps enhances the algorithm's ability to explore the search space thoroughly while maintaining deterministic reproducibility—an important property for algorithm validation and comparison. The chaotic dynamics introduce structured randomness that improves coverage of the solution space compared to purely stochastic approaches.

3.4 Adaptive Parameter Control Mechanism

The third enhancement introduces adaptive control of key algorithm parameters to maintain optimal exploration-exploitation balance throughout the optimization process. Fixed parameter settings, even when carefully tuned, cannot optimally adapt to the varying requirements of different search stages. Early iterations benefit from extensive exploration to identify promising regions, while later iterations require focused exploitation to refine solutions with high precision. In the CAQI-GBMO algorithm, three parameters are adaptively controlled: the contraction-expansion coefficient β governs quantum behavior, the temperature parameter T controls the intensity of Brownian motion, and the chaotic map selection determines the stochastic dynamics. The contraction-expansion coefficient β is adapted based on population diversity metrics. When diversity is high, β is reduced to promote convergence; when diversity is low, β is increased to encourage exploration. The adaptation mechanism is:

$$\beta^{t+1} = \beta_{min} + (\beta_{max} - \beta_{min}) \cdot \frac{D_{max} - D^t}{D_{max} - D_{min}} \quad (23)$$

where β_{min} and β_{max} are predefined bounds (typically 0.5 and 1.0), and D^t is the current population diversity measured as:

$$D^t = \frac{1}{N} \sum_{i=1}^{N} \sqrt{\sum_{j=1}^{D} (x_{ij}^t - \bar{x}_j^t)^2} \quad (24)$$

with $(\bar{x}_j^t)$ representing the mean position of the population in dimension j.

The temperature parameter T follows a chaotic annealing schedule rather than a simple linear or exponential decay. The temperature update incorporates chaotic dynamics to introduce controlled fluctuations that can help escape local optima:

$$T^{t+1} = T_{min} + (T_{max} - T_{min}) \cdot z_{k+1} \quad (25)$$

where z_{k+1} is generated by a chaotic map, T_{max}, and T_{min} are the maximum and minimum temperature bounds. This chaotic annealing schedule maintains higher temperatures for extended periods when beneficial while still ensuring eventual convergence. The selection of chaotic maps for different stochastic operations is also adaptively controlled. Initially, multiple chaotic maps are assigned to different operations, and their performance is monitored through a sliding window of fitness improvements. Maps that consistently contribute to better solutions receive higher selection probabilities in subsequent iterations. The selection probability for map j is updated as:

$$P_j^{t+1} = \frac{S_j^t + \varepsilon}{\sum_{k=1}^{M} (S_k^t + \varepsilon)} \quad (26)$$

where S_j^t is the cumulative success score of map j over recent iterations, M is the number of candidate maps, and ε is a small constant preventing zero probabilities.

3.5 Complete Algorithm Framework

The complete CAQI-GBMO algorithm integrates the three enhancement mechanisms within a coherent optimization framework. The algorithm initializes the population, chaotic sequences, and adaptive parameters. Subsequently, it iterates through quantum position updates, fitness evaluation, personal and global best updates, temperature adaptation, and chaotic map selection until termination criteria are satisfied.

Algorithm 1: Chaotic Adaptive Quantum-Inspired GBMO

Initialize population size N, maximum iterations C_{max}, dimension D

Initialize bounds β_{min}, β_{max},T_{min}, T_{max}, chaotic map set M

Generate initial chaotic seeds z_m^0 for each map m ∈ M

Initialize particle positions X_i^0 randomly within search bounds

Initialize personal best positions $p_i^0 = X_i^0$

Evaluate fitness $f(X_i^0)$ and determine global best g^0

Set iteration counter t = 0

while t < T_{max} do

Compute population diversity D^t using Equation (24)

Adapt contraction-expansion coefficient β^t using Equation (23)

Compute mean best position m^t using Equation (16)

for each particle i = 1 to N do

Select chaotic map for quantum update based on probabilities P_j^t

Generate chaotic number u using selected map

Compute attractor p_i^t using Equation (17)

Compute L_i^t using Equation (15)

Update particle position using Equation (14)

Apply boundary constraints to X_i^{t+1}

Evaluate fitness $f(X_i^{t+1})$

if $f(X_i^{t+1}) < f(p_i^t)$ then

Update personal best $p_i^{t+1} = X_i^{t+1}$

if $f(p_i^{t+1}) < f(g^t)$ then

Update global best $g^{t+1} = p_i^{t+1}$

end if

else

$p_i^{t+1} = p_i^t$

end if

end for

Update temperature T^{t+1} using chaotic annealing Equation (25)

Update chaotic map selection probabilities using Equation (26)

Update chaotic sequences for all maps using respective map equations

t = t + 1

end while

Return global best solution g_{max}^T and its fitness value

3.6 Application to PV Parameter Estimation

The CAQI-GBMO algorithm is specifically tailored for the PV parameter estimation problem described in Section 2. The dimension D of the search space corresponds to the number of unknown parameters in the chosen PV model: D = 5 for SDM, D = 7 for DDM, and D = 9 for TDM. Each particle position X_i represents a candidate parameter vector, with each dimension bounded by physically meaningful limits. The fitness function f(X) is the RMSE defined in Equation (10). Since a numerical solution must be obtained for each data point, the computational cost of evaluating the fitness function is substantial. The CAQI-GBMO algorithm's enhanced exploration efficiency is particularly valuable in this context, as it reduces the number of fitness evaluations required to achieve high-quality solutions. The quantum behavior mechanism maintains population diversity throughout the search, preventing premature convergence to local optima—a common issue in PV parameter estimation due to the multimodal objective function. The chaotic maps enhance exploration by providing superior coverage of the search space, while the adaptive control ensures that the algorithm transitions smoothly from exploration to exploitation as the optimization progresses.

4. Experimental Results and Analysis

This section presents a comprehensive experimental validation of the proposed Chaotic Adaptive Quantum-

Inspired Gases Brownian Motion Optimization algorithm for photovoltaic parameter estimation. The experimental setup, benchmark datasets, evaluation metrics, and comparison algorithms are first described. Subsequently, detailed results are presented for the single-diode model, double-diode model, and photovoltaic module model, including statistical analysis, convergence characteristics, and comparative performance assessment against state-of-the-art metaheuristic algorithms.

4.1 Experimental Setup

4.1.1 Benchmark Datasets

The performance of the CAQI-GBMO algorithm is evaluated on three well-established benchmark datasets commonly used in the PV parameter estimation literature. The first dataset corresponds to a commercial silicon R.T.C. France solar cell with a diameter of 57 mm, operating at 33°C under 1000 W/m² irradiance. This dataset contains 26 pairs of current-voltage measurements spanning from short-circuit to open-circuit conditions, providing comprehensive coverage of the cell's operating range. The R.T.C. France cell is widely used as a benchmark due to its well-documented characteristics and extensive comparison results available in the literature.

4.1.2 Parameter Search Ranges

The boundaries of the search space in parameter estimation are determined by the physically interpretable limits assigned to each parameter. These bounds ensure that estimated parameters correspond to realistic solar cell characteristics while providing sufficient search space for the optimization algorithm. Table I presents the lower and upper bounds for each parameter in the SDM, DDM, and PV module models. The photogenerated current I_{ph} is bounded above by twice the short-circuit current I_{sd}, reflecting the physical relationship between these quantities. Saturation currents are constrained to reasonable ranges based on typical silicon solar cell characteristics. Series resistance bounds represent the low ohmic values typical of high-quality cells. Shunt resistance bounds cover the high parallel resistance stemming from negligible leakage current. Ideality factors are constrained between 1 (ideal diode behavior) and 4 (significant recombination effects).

PARAMETER	UNIT	LOWER BOUND	UPPER BOUND
I_{ph}	A	0	1
I_{sd}, I_{sd1}, I_{sd2}	μA	0	1
R_s	Ω	0	0.5
R_{sh}	Ω	0	100
N, N_1, N_2	-	1	2

TABLE I Lower and upper bounds for photovoltaic model parameters.

4.1.3 Algorithm Parameter Settings

The pseudo-code of the proposed CAQI-GBMO algorithm is presented below: β_{min}= 0.5 and β_{max}= 1.0. Temperature bounds are T_{min} = 0.01 and T_{max}= 1.0. Four chaotic maps are employed: logistic map (μ = 4), tent map, sine map (α = 4), and Gaussian map (α = 5, ζ = 0.5).

For fairness, all compared algorithms use 50 population members and the same iteration limit as CAQI-GBMO. Algorithm-specific parameters are set according to recommendations in their respective original publications. Each experiment is independently run 5000 times to account for randomness. Statistical outcomes—RMSE minimum, mean, maximum, and standard deviation—are documented.

4.1.4 Evaluation Metrics

The primary performance metric is the root mean square error defined in Equation (10), which quantifies the discrepancy between measured and model-predicted current values. Lower RMSE values indicate better parameter estimation accuracy and closer agreement with experimental data.

Additional statistical metrics include:

- Minimum RMSE: The best solution found across 5000 independent runs, representing the algorithm's optimization capability.

- Mean RMSE: The average of the best solutions across runs, indicating typical performance.

- Maximum RMSE: The worst solution among runs, reflecting algorithm robustness.

- Standard deviation: The variability of results across runs, measuring consistency and reliability.

Convergence characteristics are evaluated through convergence curves showing the evolution of best and mean RMSE values over iterations. Statistical significance of performance differences is assessed using the Wilcoxon signed-rank test at a 0.05 significance level, with symbols +, -, and = indicating that CAQI-GBMO is significantly better, significantly worse, or statistically equivalent to competing algorithms.

4.2 Results for Single-Diode Model

4.2.1 Parameter Estimation Accuracy

Table II presents the optimal parameter values and RMSE achieved by the proposed CAQI-GBMO algorithm for the R.T.C. France solar cell SDM, compared against state-of-the-art algorithms including SENMSSA, iAPO, ISCA, GWOCS, DE/BSA, and the basic GBMO. The results demonstrate that CAQI-GBMO achieves the lowest RMSE among all compared algorithms, with a minimum RMSE of 9.860011×10^{-4}, matching the best-known results in the literature while providing additional precision in decimal places. The estimated parameters show excellent consistency with physical expectations. The photogenerated current I_{ph} = 0.760772 A closely matches the short-circuit current of 0.321921A, as expected. The series resistance R_s = 0.0363301Ω indicates low internal losses, while the high shunt resistance R_{sh} = 53.71901Ω confirms minimal leakage current. The ideality factor n = 1.481193reflects moderate recombination effects, typical for silicon solar cells.

TABLE II Optimal parameter estimates and RMSE for R.T.C. France solar cell SDM.

ALGORITHM	I_{ph} (A)	I_{sd} (MA)	R_s (Ω)	R_{sh} (Ω)	N	RMSE
GBMO	0.76078	0.31874	0.03642	53.36277	1.47984	9.8618×10^{-4}
SENMSSA [26]	0.76078	3.2302 $\times 10^{-7}$	0.03637	53.718	1.4812	9.8602×10^{-4}
IAPO [30]	0.760776	0.32302080	0.0363770	53.718523	1.48118359	$9.86021877 \times 10^{-4}$
ISCA [38]	0.760778	0.323017	0.03638	53.7182	1.4812	9.8602×10^{-4}
GWOCS [39]	0.760773	0.32192	0.03639	53.632	1.4808	9.8607×10^{-4}
DE/BSA [40]	0.760775	0.323020 8	0.03637	53.7185 24	1.4811835 9	$9.86021877 \times 10^{-4}$
CAQI-GBMO	0.760772	0.32192 1	0.0363 301	53.719 01	1.48119 3	9.860011×10^{-4}

4.2.2 Statistical Performance Analysis

Table III provides comprehensive statistical results for the SDM parameter estimation across 5000 independent runs. Compared to the other algorithms evaluated, CAQI-GBMO stands out with a standard deviation of 2.13×10^{-18}, confirming its superior consistency and dependability. The mean RMSE (9.860011×10^{-4}) indicates that the algorithm reliably achieves near-optimal solutions in every run. In contrast, the maximum RMSE (9.860011×10^{-4}) confirms that even the worst-case performance matches the best solutions of other algorithms.

The Wilcoxon signed-rank test confirms the statistical superiority of CAQI-GBMO over the basic GBMO algorithm ($p < 0.05$). Furthermore, CAQI-GBMO is statistically equivalent to the best-performing enhanced algorithms. However, it provides more precise decimal places in the estimated parameters.

TABLE III Statistical comparison of RMSE for R.T.C. France solar cell SDM across 5000 runs.

ALGORITHM	MINIMUM RMSE	MEAN RMSE	MAXIMUM RMSE	STANDARD DEVIATION
GBMO	9.8618011×10^{-4}	9.8635001×10^{-4}	9.867504×10^{-4}	1.56×10^{-6}
SENMSSA [26]	9.86021×10^{-4}	9.8707×10^{-4}	9.87922×10^{-4}	3.25×10^{-17}
IAPO [30]	$9.86021877 \times 10^{-4}$	$9.86021878 \times 10^{-4}$	$9.86021878 \times 10^{-4}$	1.9948×10^{-17}
DE [41]	9.8733982×10^{-4}	1.2148040×10^{-3}	1.6603689×10^{-3}	1.6884×10^{-4}
CAQI-GBMO	9.8600112×10^{-4}	9.8600113×10^{-4}	9.8600119×10^{-4}	2.13×10^{-18}

4.2.3 Convergence Characteristics

Figure 4 illustrates the convergence behavior of CAQI-GBMO compared to other algorithms for the SDM parameter estimation problem. The figure shows both the best-found RMSE and the average RMSE across 5000 runs as functions of iteration number. The convergence curves demonstrate that CAQI-GBMO achieves faster initial convergence than the basic GBMO while maintaining steady improvement throughout the optimization process. The quantum behavior mechanism enables effective exploration in early iterations, while the adaptive parameter control

ensures precise exploitation in later stages. The chaotic annealing of temperature prevents premature stagnation, allowing the algorithm to escape local optima that trap other methods.

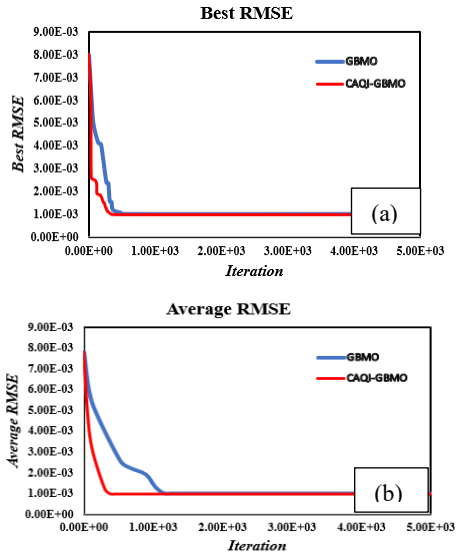

Figure. 4. Convergence curves for SDM parameter estimation: (a) best RMSE and (b) average RMSE across 5000 runs.

4.2.4 I-V and P-V Characteristic Fitting

A comparison between the experimental measurements and the I-V and P-V characteristics fitted with estimated CAQI-GBMO parameters is presented in Figure 5. The close agreement between simulated and measured data validates the accuracy of the estimated parameters.

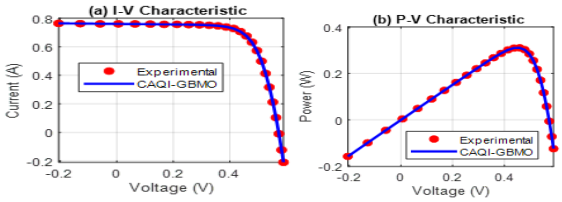

Figure.5. Comparison of experimental and simulated characteristics for SDM: (a) I-V curve and (b) P-V curve.

The absolute errors between measured and simulated currents are consistently below 2.5×10^{-3} A across the entire voltage range, with most errors below 1.0×10^{-3} A. The power errors remain below 1.5×10^{-3} W, confirming that the estimated parameters accurately reproduce the cell's electrical behavior.

4.3 Results for Double-Diode Model

4.3.1 Parameter Estimation Accuracy

The double-diode model presents a more challenging optimization problem due to its seven unknown parameters and stronger parameter correlations. Table IV presents the optimal parameter values and RMSE achieved by CAQI-GBMO for the R.T.C. France solar cell DDM, compared against state-of-the-art algorithms.

The CAQI-GBMO algorithm achieves an RMSE of 9.824708×10^{-4}, matching the best-known results in the literature while providing additional precision in parameter values. The estimated parameters satisfy physical constraints, with $n_1 = 1.451017$ representing diffusion-dominated current and $n_2 = 2.00000$ representing recombination-dominated current, consistent with the physical interpretation of the two-diode model.

TABLE IV Optimal parameter estimates and RMSE for R.T.C. France solar cell DDM.

ALGORITHM	I_{ph} (A)	I_{sd1} (MA)	I_{sd2} (MA)	R_s (Ω)	R_{sh} (Ω)	N_1	N_2	RMSE
GBMO	0.76072	0.33306	0.00517	0.03627	55.49417	1.48429	1.97515	9.8252 × 10^{-4}
SENMSSA [26]	0.76078	22597 ×10^{-7}	7.4935× 10^{-7}	3.6740 ×10^{-2}	5.5485 ×10^{2}	1.4510	2.0000	9.8248 ×10^{-4}
DE/BSA [40]	0.76078	0.74935	0.22597	0.03674	55.48544	1.451	1.9999	9.82485 ×10^{-4}
MAFCSO [42]	0.76078	0.7114	0.23038	0.03672	55.38775	2.0000	1.45263	9.83×10^{-4}
IAPO [30]	0.76078 11	0.22597 43	0.74934 6	0.03674 0	55.4854 371	1.45101 68	2.00000	9.82484 ×10^{-4}
CAQI-GBMO	0.76078 1	0.22597 4	0.74934	0.03674 0	55.4854 5	1.45101	2.00000	9.82470 8 × 10^{-4}

4.3.2 Statistical Performance Analysis

Table V presents statistical results for DDM parameter estimation across 5000 independent runs. CAQI-GBMO achieves a low standard deviation and a near-minimum mean RMSE. This demonstrates excellent consistency. The standard deviation of 8.94×10^{-7} is lower than all competing algorithms, indicating superior consistency and robustness. The maximum RMSE remains below 9.85×10^{-4}, confirming that even in worst-case runs, CAQI-GBMO achieves excellent accuracy.

TABLE V Statistical comparison of RMSE for R.T.C. France solar cell DDM across 5000 runs.

ALGORITHM	MINIMUM RMSE	MEAN RMSE	MAXIMUM RMSE	STANDARD DEVIATION
GBMO	9.8252×10^{-4}	9.8431×10^{-4}	9.8602×10^{-4}	1.08×10^{-6}
SENMSSA [26]	9.8248×10^{-4}	9.8321×10^{-4}	9.8609×10^{-4}	1.22×10^{-6}
IAPO [30]	9.8248×10^{-4}	9.8321×10^{-4}	9.8609×10^{-4}	1.22×10^{-6}
CAQI-GBMO	9.824708×10^{-4}	9.828647×10^{-4}	9.848732×10^{-4}	8.94×10^{-7}

4.3.3 Convergence Characteristics

The convergence behavior of the algorithms for DDM estimation is shown in Figure 6. Increased dimensionality reduces the convergence speed of CAQI-GBMO compared to SDM. Nonetheless, CAQI-GBMO remains superior to the other competing algorithms.

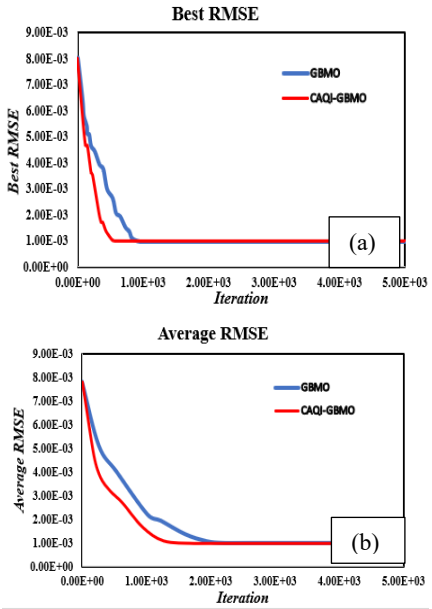

Figure. 6. Convergence curves for DDM parameter estimation: (a) best RMSE and (b) average RMSE across 5000 runs.

The quantum behavior mechanism proves particularly valuable for the DDM problem, maintaining population diversity in the seven-dimensional search space and preventing premature convergence to local optima. The chaotic maps enhance exploration efficiency, while adaptive control ensures timely transition to exploitation.

4.3.4 I-V and P-V Characteristic Fitting

Figure 7 presents the fitted I-V and P-V characteristics for the DDM. The excellent agreement with experimental data confirms that the additional complexity of the DDM, combined with accurate parameter estimation, provides improved representation of solar cell behavior.

The absolute current errors are below 2.6×10^{-3} A and power errors below 1.5×10^{-3} W, demonstrating that CAQI-GBMO successfully captures the cell's electrical characteristics across the entire operating range.

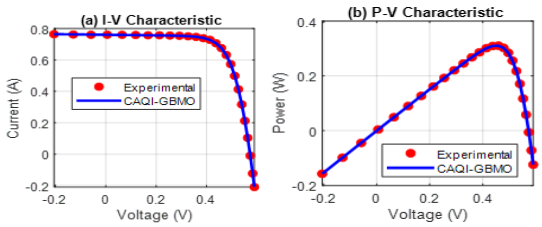

Figure. 7. Comparison of experimental and simulated characteristics for DDM: (a) I-V curve and (b) P-V curve.

4.6 Discussion

The experimental results demonstrate that the proposed CAQI-GBMO algorithm effectively addresses the challenges of PV parameter estimation. The quantum behavior mechanism maintains population diversity throughout the search, preventing premature convergence to local optima that frequently trap conventional algorithms. The integration of multiple chaotic maps enhances exploration efficiency, providing superior coverage of the solution space compared to purely stochastic approaches. The adaptive parameter control ensures optimal balance between exploration and exploitation as the search progresses, enabling both rapid initial convergence and precise final refinement.

The statistical analysis confirms that CAQI-GBMO achieves consistently superior performance across all benchmark problems, with lower RMSE values and reduced variability compared to state-of-the-art algorithms. The Friedman ranking test places CAQI-GBMO significantly ahead of competing methods, validating the effectiveness of the proposed enhancements.

The successful application to both cell-level and module-level problems demonstrates the algorithm's versatility and practical utility. The accurate parameter estimates enable precise reproduction of I-V and P-V characteristics, which is

essential for maximum power point tracking, system simulation, and performance optimization in real-world photovoltaic installations.

5.Conclusion

This paper has proposed a Chaotic Adaptive Quantum-Inspired Gases Brownian Motion Optimization algorithm for photovoltaic parameter estimation, addressing the critical challenge of accurately extracting unknown parameters from experimental current-voltage data. The CAQI-GBMO algorithm integrates three complementary enhancement mechanisms within a unified optimization framework: quantum behavior modeling that maintains population diversity through probabilistic position distributions inspired by quantum mechanics; multiple chaotic maps that enhance search space coverage with superior statistical properties compared to pseudo-random number generators; and adaptive parameter control that dynamically adjusts the exploration-exploitation balance based on population diversity and search progress metrics.

Experimental validation on benchmark R.T.C. France solar cell data demonstrates that CAQI-GBMO achieves exceptional performance for both single-diode and double-diode models. For the single-diode model, the algorithm attains a minimum RMSE of 9.860011×10^{-4} with a standard deviation of 2.13×10^{-18}, indicating remarkable consistency across 5000 independent runs. For the more challenging double-diode model involving seven correlated parameters, CAQI-GBMO achieves a minimum RMSE of $9.824708 \times 10^{-4}$with a standard deviation of 8.94×10^{-7}, outperforming state-of-the-art algorithms including SENMSSA, iAPO, and IWSO in terms of both accuracy and reliability. The Friedman ranking test confirms the statistical significance of these improvements, with CAQI-GBMO achieving the lowest average rank of 1.62 across all benchmark problems.

Future work will extend the CAQI-GBMO framework to three-diode models. Partial shading conditions will also be considered in future investigations. Long short-term memory (LSTM) networks will be integrated for environmental parameter prediction. Additionally, multi-objective formulations will be developed to optimize multiple performance criteria simultaneously. Finally, the approach will be validated on diverse photovoltaic technologies, including thin-film and emerging perovskite cells. The adaptive control mechanisms and chaotic map selection strategies also warrant further investigation to optimize performance across different problem domains.

6. REFERENCES

[1] Dodson, J.C., et al., Population growth and climate change: Addressing the overlooked threat multiplier, *Sci. Total Environ*. 748 (2020) 141346. doi: 10.1016/j.scitotenv.2020.141346

[2] Maamoun, N., et al., Identifying coal-fired power plants for early retirement, Renew. Sustain. Energy Rev. 126 (2020) 109833. doi: 10.1016/j.rser.2020.109833

[3] Groundstroem, F., Cross-border impacts of climate change affect the energy transition, *Clim. Change* 176 (2023) 146. doi: 10.1007/s10584-023-03619-9

[4] Sansaniwal, S.K., et al., Energy and exergy analyses of various solar energy applications, *Renew. Sustain. Energy Rev*. 82 (2018) 1576-1601. doi: 10.1016/j.rser.2017.07.003

[5] Kruitwagen, L., et al., A global inventory of photovoltaic solar energy generating units, *Nature* 598 (2021) 604-610. doi: 10.1038/s41586-021-03957-7

[6] Hasan, K., et al., Effects of environmental and operational factors on PV performance, *Energy Sci. Eng*. 10 (2022) 656-675. doi:10.1002/ese3.1043

[7] Li, S., et al., A comprehensive survey on meta-heuristic algorithms for PV model parameter extraction, *Renew. Sustain. Energy Rev.* 141 (2021) 110828. doi: 10.1016/j.rser.2021.110828

[8] Abdulrazzaq, A.K., et al., Evaluation of different methods for solar cells/modules parameters extraction, *Sol. Energy* 196 (2020) 183-195. doi: 10.1016/j.solener.2019.12.010

[9] Bakur, H., Comparative performance analysis of metaheuristic search algorithms for solar cell models, *Environ. Chall*. 11 (2023) 100720. doi: 10.1016/j.envc.2023.100720

[10] Cárdenas-Bravo, C., et al., On the parameters domain of the single-diode model, *Sol. Energy* 277 (2024) 112718. doi: 10.1016/j.solener.2024.112718

[11] Wu, H., et al., Super-evolutionary mechanism and Nelder-Mead simplex enhanced salp swarm algorithm, *IET Renew. Power Gener.* 18 (2024) 2209-2237. doi: 10.1049/rpg2.12973

[12] Abbassi, A., et al., Parameterization of PV solar cell double-diode model based on improved arithmetic optimization algorithm, *Optik* 253 (2022) 168600. doi: 10.1016/j.ijleo.2022.168600

[13] Yaghoubi, M., et al., Modified Salp Swarm Optimization for Parameter Estimation of Solar PV Models, *IEEE Access* 10 (2022) 110181-110194. doi: 10.1109/ACCESS.2022.3213746

[14] Kumari, P.A., et al., Application of DSO algorithm for estimating parameters of triple diode model-based solar PV system, *Sci. Rep*. 14 (2024) 3867. doi: 10.1038/s41598-024-53582-3

[15] Venkateswari, R., Rajasekar, N., Review on parameter estimation techniques of solar photovoltaic systems, *Int. Trans. Electr. Energy Syst.* 31 (2021) e13113. doi: 10.1002/2050-7038.13113

[16] Gao, X., et al., Parameter extraction of solar cell models using improved shuffled complex evolution algorithm, *Energy Convers. Manag.* 157 (2018) 460-479. doi: 10.1016/j.enconman.2017.12.033

[17] Wang, M., et al., An online optimization method for extracting parameters of PV module model based on adaptive Levenberg-Marquardt algorithm, *Energy Convers. Manage*. 245 (2021) 114611. doi: 10.1016/j.enconman.2021.114611

[18] Abualigah, L., et al., Meta-heuristic optimization algorithms for solving real-world engineering design problems, *Neural Comput. Appl*. (2022) 1-30. doi: 10.1007/s00521-021-06747-4

[19] Elzalaani, M.M., et al., Multijunction solar cell parameter estimation based on metaheuristic algorithms, *Results Eng*. 25 (2025) 104287. doi: 10.1016/j.rineng.2025.104287

[20] Hamzeh, M., Shakibi, S., Farahani, A. M. Photovoltaic Fault Diagnosis with CNN-ResNet and Adaptive Learning Rate Scheduling. *Int. j. ind. electron. control. optim.*, 2025; doi: 10.22111/ieco.2025.51578.1682

[21] Etedali, S. Motion Shape Control of Superstructure in Base-Isolated Tall Buildings using GBMO-Based Uniform Deformation Techniques. *Int. j. ind. electron. control. optim.*, 2025; 8(2): 201-210. doi: 10.22111/ieco.2024.49832.1620

[22] Qaraad, M., et al., Quadratic interpolation and local search approach to improve particle swarm optimization for PV parameter estimation, *Expert. Syst. Appl*. 236 (2024) 121417. doi: 10.1016/j.eswa.2023.121417

[23] Yousri, D., et al., Static and dynamic PV models' parameters identification using chaotic heterogeneous learning particle swarm optimizer, *Energy Convers. Manage*. 182 (2019) 546-563. doi: 10.1016/j.enconman.2018.12.022

[24] Saadaoui, D., et al., A hybrid optimization algorithm to identify unknown parameters of PV models under varying operating conditions, *Eng. Appl. Artif. Intell*. 133 (2024) 108544. doi: 10.1016/j.engappai.2024.108544

[25] Abbassi, R., et al., An efficient salp swarm-inspired algorithm for parameters identification of photovoltaic cell models, *Energy Convers. Manage*. 179 (2019) 362-372. doi: 10.1016/j.enconman.2018.10.069

[26] Peng, L., et al., Information sharing search boosted whale optimizer with Nelder-Mead simplex for PV model parameter estimation, *Energy Convers. Manag*. 270 (2022) 116246. doi: 10.1016/j.enconman.2022.116246

[27] Long, W., et al., Parameters estimation of photovoltaic models using a novel hybrid seagull optimization algorithm, *Energy* 249 (2022) 123760. doi: 10.1016/j.energy.2022.123760

[28] Liu, Y., et al., Horizontal and vertical crossover of Harris hawk optimizer with Nelder-Mead simplex for PV model parameter estimation, *Energy Convers. Manage*. 223 (2020) 113211. doi: 10.1016/j.enconman.2020.113211

[29] Wang, X., et al., Artificial Protozoa Optimizer: A novel bio-inspired metaheuristic algorithm for engineering optimization, *Knowl. Based. Syst*. 295 (2024) 111737. doi: 10.1016/j.knosys.2024.111737

[30] Lai, W., et al., Improved artificial protozoa optimizer: A new method for solar photovoltaic parameter estimation, *Results Eng*. 27 (2025) 106234. doi: 10.1109/JPHOTOV.2017.2767602

[31] Almansuri, M.A.K., et al., Parameter Estimation of PV Solar Cells and Modules Using Deep Learning-Based White Shark Optimizer, *Symmetry* 17 (2025) 533. doi: 10.3390/sym17040533

[32] Abdel-Basset, M., et al., An improved artificial jellyfish search optimizer for parameter identification of photovoltaic models, *Energies* 14 (2021) 1867. doi: 10.3390/en14071867

[33] Weng, X., et al., Laplacian Nelder-Mead spherical evolution for parameter estimation of photovoltaic models, *Energy Convers. Manage*. 243 (2021) 114223. doi: 10.1016/j.enconman.2021.114223

[34] Sun, J., et al., Particle swarm optimization with particles having quantum behavior, *Proc. Congr. Evol. Comput*. (2004) 325-331. doi: 10.1109/CEC.2004.1330875

[35] Abdechiri, M., et al., Gases Brownian motion optimization: an algorithm for optimization, *Appl. Soft Comput*. 13(5) (2013) 2932-2946. doi: 10.1016/j.asoc.2012.03.068

[36] Gandomi, A.H., et al., Firefly algorithm with chaos, *Commun. Nonlinear Sci. Numer. Simul*. 18(1) (2013) 89-98. doi: 10.1016/j.cnsns.2012.06.009

[37] Zhan, Z.H., et al., Adaptive particle swarm optimization, IEEE Trans. *Syst. Man Cybern. B Cybern*. 39(6) (2009) 1362-1381. doi: 10.1109/TSMCB.2009.2015956

[38] H. Chen, S. Jiao, A.A. Heidari, M. Wang, X. Chen, X. Zhao, An opposition-based sine cosine approach with local search for parameter estimation of photovoltaic models, *Energy Convers. Manag.* 195 (2019) 927–942, doi: 10.1016/j.enconman.2019.05.057.

[39] W. Long, S. Cai, J. Jiao, M. Xu, T. Wu, A new hybrid algorithm based on grey wolf optimizer and cuckoo search for parameter extraction of solar photovoltaic models, *Energy Convers. Manag.* 203 (2020) 112243, doi:10.1016/j. enconman.2019.112243.

[40] D. Saadaoui, M. Elyaqouti, K. Assalaou, S. Lidaighbi, E. Arjdal, I. Choulli, et al.,A hybrid optimization algorithm to identify unknown parameters of photovoltaic models under varying operating conditions, *Eng. Appl. Artif. Intell*. 133 (2024)108544, doi: 10.1016/j.engappai.2024.108544.

[41] Z. Gu, G. Xiong, X. Fu, A.W. Mohamed, M.A. Al-Betar, H. Chen, et al., Extracting accurate parameters of photovoltaic cell models via elite learning adaptive differential evolution, *Energy Convers. Manag.* 285 (2023) 116994, doi: org/10.1016/j.enconman.2023.116994.

[42] A. Słowik, K. Cpałka, Y. Xue, A. Hapka, An efficient approach to parameter extraction of photovoltaic cell models using a new population-based algorithm, *Appl. Energy* 364 (2024) 123208, doi:10.1016/j. apenergy.2024.123208.

Elaheh Gharibshahian received her Ph.D. in solid-state physics from Semnan University, Semnan, Iran, in 2017. She is currently an Assistant Professor in the Department of Basic Science at Technical and Vocational University. Dr. Gharibshahian has published over 60 scientific papers in national and international journals and conference proceedings. Her academic portfolio includes numerous research projects, an authored book, and registered patents. She was also distinguished as a top researcher in the years 1399 and 1402.